

Learning Scalable Self-Driving Policies for Generic Traffic Scenarios

Peide Cai, Hengli Wang, Yuxiang Sun, and Ming Liu, *Senior Member, IEEE*

Abstract—Robust and safe self-driving in complex and dynamic environments is quite challenging due to the requirement of scalable driving policies against the wide variety of traffic scenarios (e.g., road topologies, traffic rules and interaction with road agents). In this area, traditional modular frameworks scale poorly in new environments, and require tremendous and iterative hand-tuning of rules and parameters to maintain performance in all foreseeable scenarios. Recently, deep-learning based self-driving methods have shown promising results with better generalization capability but less hand engineering effort. However, most of the previous methods are trained and evaluated in limited and simple environments with scattered tasks, such as lane-following, autonomous braking and conditional driving. In this paper, we propose a graph-based deep network to achieve unified and scalable self-driving in diverse dynamic environments. The extensive evaluation results show that our model can safely navigate the vehicle in a large variety of urban, rural, and highway areas with dense traffic while obeying traffic rules. Specifically, more than 7,500 km of closed-loop driving evaluation is conducted in dynamic simulation environments, in which our method can handle complex driving situations, and achieve higher success rates (73.5%-83.2%) and driving scores than the baselines.

I. INTRODUCTION

Decision, planning and control for self-driving vehicles (SDVs) in complex and dynamic urban environments are quite challenging. For one thing, there are diverse road topologies, geometries and scenarios (e.g., roundabouts, multi-lane streets and intersections) to consider [1]. For another, the complex and coupled interaction among multiple road agents (e.g., pedestrians, bicyclists and vehicles) are hard to model [2]. Besides these, various traffic rules should also be obeyed, such as traffic light, lane markings and speed limit.

Classical methods use priors and domain knowledge to decompose the self-driving task into a modular and sequential pipeline [3], [4]. For example, based on the perception results, a popular pipeline is: 1) scenario-based high level decision, 2) trajectory prediction of surrounding obstacles, and 3) motion planning and control [5], [6]. However, the main drawback of these approaches is the difficulty to generalize in new scenarios, thus they require time-intensive and iterative hand tuning of rules and parameters to maintain performance [7]. Further common problems are the occurrence of local minima [8] and oscillations [9].

In recent years, as an alternative way, deep learning has advanced the SDV technology to a great extent. The ability to *learn and self-optimize* its behavior from data makes a deep driving model well suited to decision and control

All authors are with The Hong Kong University of Science and Technology (email: {pcaiaa,hwangdf,ceyxsun,eelium}@ust.hk).

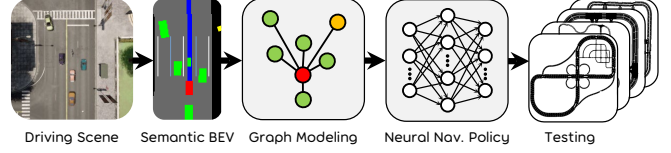


Fig. 1. A deep navigation policy is learned with graph neural networks. The resulting policy is tested extensively in multiple maps covering urban, rural and highway scenarios.

problems in high-dimensional, nonlinear and dynamic environments [10]–[19], which is free from explicit modeling of all foreseeable scenarios and laborious engineering maintenance. However, current learning models have not been well designed for scalable self-driving in a uniform setup. Specifically, most works only focus on scattered tasks such as lane-following [20], [21], lane-changing [22], collision avoidance [23]–[26], or simple conditional urban driving [12], [13], [16]–[19]. In short, robust and high-performance models still seem out of reach [10].

To solve the aforementioned problem, in this paper we propose a deep network for end-to-end decision, planning and control to achieve scalable self-driving, named DiGNet (driving in graphs). Specifically, as shown in Fig. 1, we use graph attention networks (GAT) [27] to model the complex interactions among traffic agents, use semantic bird’s-eye view (BEV) images to model road topologies and traffic rules, and adopt the variational auto-encoder (VAE) [28] to extract effective and interpretable environmental features. The main contributions of this paper are as follows.

- A specially designed network architecture for self-driving in generic traffic environments considering traffic rules (e.g., speed limit and traffic light) and interaction among multiple dynamic road agents (e.g., collision avoidance in vehicle- and pedestrian-rich environments).
- Scalable and safe self-driving performance demonstrated in both seen and unseen urban/rural/highway environments by extensive evaluation in a high-fidelity driving simulation.

II. RELATED WORK

A. Imitation Learning (IL)

IL has been the most preferred approach in the community for learning-based vehicle control due to its sample efficiency [10]. For this method, each data point in the training set includes an observation-action pair. During training, the deep network compares the action error between its prediction and the expert labelled data, then adjust its weights using gradient descent. Based on large amount of expert labelled data, *end-to-end* driving approaches [11], [12], [16], [18],

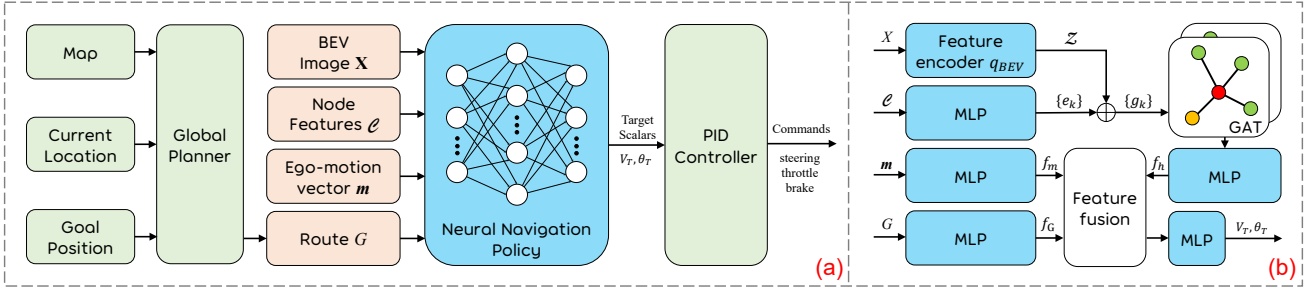


Fig. 2. (a) Schematic overview of the proposed method for self-driving. (b) The data flow inside the neural navigation network (DiGNet).

[21] take as input the raw sensor readings (e.g., LiDAR point clouds, camera images) to directly output control commands such as steering angle and throttle, which imitates human behaviors. For example, Xu *et al.* [21] develop an end-to-end architecture to predict future vehicle egomotion from a large-scale video dataset. However, this work only targets lane-following tasks and lacks closed-loop experiments. Codevilla *et al.* [16] propose a conditional imitation learning approach that splits the network into multiple branches for discrete tasks: follow lane, turn left, turn right and keep straight at intersections. Follow-up works include [12], [17] and [18]. However, this method cannot handle complex road topologies such as multi-lane streets or roundabouts. Recently, Cai *et al.* [11] use global routes as direction and multi-modal sensor input to achieve robust end-to-end navigation in complex dynamic environments. The drawback of this work is the neglect of both traffic rules and efficient interaction with other road agents (e.g., overtaking a vehicle blocked ahead).

To conclude, it is quite challenging to learn a direct mapping from high dimensional sensory observations to low dimensional control output, which not only requires a large amount of labelled data to constrain the learning process, but also suffer from the inherent domain gap problem [29]. To alleviate this, recently, there arises another framework that uses intermediate representations to learn driving policies, such as HD maps [1], [30], pre-processed birdseye views (BEVs) of the surroundings [15] and semantic occupancy maps [31]. Compared with the sensory observations which are quite redundant [32], these BEV-based input representations are both concise and informative, making the learning process much more efficient. For example, ChauffeurNet [15] takes as input hybrid features composed of roadmap, traffic light, route plans and dynamic objects to produce waypoints to follow. This has the advantage to help the network learn meaningful contextual cues behind the human driver's action and achieve more complex driving behaviors. However, as with other similar works [30], [31], its performance is mainly shown on *logged data* with insufficient closed-loop online evaluation at scale. Actually, [15] only test simple driving tasks online, such as lane-following and turning in static environments. Our input representation is similar to that of ChauffeurNet but differently, we focus more on dynamic, interactive and large-scale *closed-loop* driving performance.

B. Graph Representation Learning

Many real-world problems can be modeled with graphs where the nodes contain features of different entities, and edges represent interactions between entities. A challenge in learning on graphs is to find an effective way to get a meaningful aggregated feature representation to facilitate downstream tasks. Recently, graph convolutional networks (GCNs) [33] have shown to be effective in many applications such as social networks, personalized recommendation and link prediction. GCN generalizes the 2D convolution on grids to graph-structured data. When training a GCN, a fixed adjacency matrix is commonly adopted to aggregate feature information of neighboring nodes. On the other hand, graph attention network (GAT) [27] is a GCN variant which aggregates node information with weights learned in a self-attention mechanism. Such adaptiveness of GAT makes it more effective than GCN in graph representation learning.

Recently, these graph neural networks (GNNs) have also been shown to be effective in robotics such as crowd robot navigation [2], [34], [35], where the robot can navigate safely in human crowds with various sizes. However, these works totally neglect the environmental structures, which is not that important for indoor robot navigation in restricted areas, but is non-negligible for outdoor self-driving problems where traffic rules should be strictly obeyed, such as driving on correct lanes. In this work, we model the traffic scenes as graphs and use a context-aware GAT to achieve autonomous vehicle navigation.

III. FORMULATION

Fig. 2 shows the structure of the proposed DiGNet for scalable self-driving. The goal is to drive safely and agilely in a large variety of complex and dynamic outdoor environments for point-to-point navigation. To this end, we use GAT to model the complicated interactions among road agents, and BEV images to represent various road structures. In addition, our system is trained and evaluated on the open-source CARLA simulation (0.9.9) [36], which is developed for autonomous driving research and provides high-fidelity dynamic world and various vehicles/pedestrians of realistic physics/behaviors.

A. Driving Scene Representation

In order to learn good driving policies, we use semantic BEV images as the representation of driving scenes to reduce

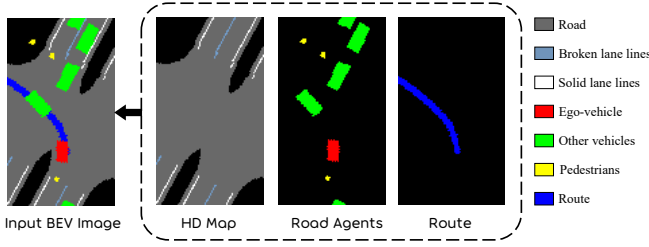


Fig. 3. BEV representation as one of the input to our network, which includes information of HD map, road agents, routes and traffic light.

the high-dimensionality and redundancy of raw sensory data. Furthermore, with such representation, there is no domain difference between the simulation and real world, thus the policy transfer problem [37] can be alleviated. Specifically, we rasterize different semantic elements (e.g., lane marking, obstacles) into multiple binary channels to form a concise and informative scene representation. As shown in Fig. 3, our BEV input is composed of the following three parts with seven channels in total:

- **High-definition (HD) Map:** The HD map contains the drivable area and lane markings (solid and broken lines). Leveraging map information to learn driving policies is very helpful because it provides valuable structural priors on the motion of surrounding road agents. For example, vehicles normally drive on lanes rather than on sidewalks. Another benefit is that vehicles need to drive according to traffic rules, such as not crossing solid lane markings.
- **Routes and Traffic Light:** The route is provided by a global planner implemented with A^* . The route channel will be set to blank when the traffic light that effects the ego-vehicle turns to red, otherwise it maintains its normal value.
- **Road Agents:** We render the ego-vehicle, other vehicles and pedestrians in three other channels.

In this work, our region of interest is $W=20$ m wide (10 m to each side of the ego-vehicle) and $H=35$ m long (25 m front and 10 m behind of the ego-vehicle). The image resolution is set to 0.25 m/pixel, which finally results in a binary BEV input \mathbf{X} of size $80 \times 140 \times 7$, which is always anchored at the ego-vehicle's current position.

B. Data Collection

We collect a dataset of 260 expert driving episodes in CARLA, which lasts about 7.6 hours and covers a driving distance of 150 km. For each data collection episode, we set random routes ranging from 300 m to 1500 m in four maps of CARLA: Town03, Town05, Town06 and Town07. These maps includes urban, rural and highway scenarios. We also set roaming pedestrians and vehicles to construct dynamic environments, which are controlled by the AI engine of CARLA.

IV. METHODOLOGY

A. Learning the Context Embedding

Although we replace the complex raw sensor data with more informative and concise BEV semantic masks, it is still

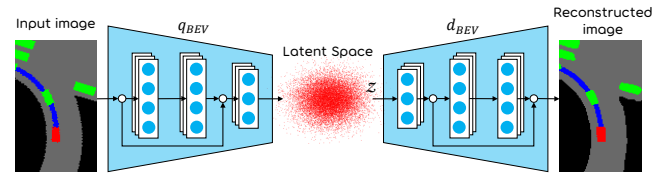


Fig. 4. VAE architecture. The input image is encoded into a latent space, from which the sampled vector \mathbf{z} can be decoded back into a reconstructed image similar to the input. Therefore, \mathbf{z} summarizes the key geometrical properties of environments.

quite high-dimensional compared to the vehicle state variables (e.g., speed, location, etc.). Such high-dimensionality makes it not only hard to learn good policies in data scarce tasks, but also suffer from over-fitting problems. Therefore, a lower-dimensional embedding for the multi-channel BEV input is needed for us to train a high-performance driving policy. To this end, following [13], [38], we first train a variational autoencoder (VAE) on the collected BEV images from Section III-B. As shown in Fig. 4, this method can help to summarize the key geometrical properties of environments in a low-dimensional latent vector \mathbf{z} , which provides interpretation of downstream tasks such as self-driving. Specifically, we adopt the β -VAE [39] and minimize the variational lower bound with encoder q_{BEV} and decoder d_{BEV} :

$$\mathcal{L}_{VAE} = \beta \cdot D_{KL}(q_{BEV}(\mathbf{z} | \mathbf{X}) || p(\mathbf{z})) + \|d_{BEV}(\mathbf{z}) - \mathbf{X}\|_2^2, \quad (1)$$

where $D_{KL}(\cdot)$ is the Kullback-Leibler (KL) divergence. The encoder $q_{BEV}(\mathbf{z} | \mathbf{X})$ takes as input the raw image and returns the mean μ and variance σ^2 of a normal distribution, such that $\mathbf{z} \sim \mathcal{N}(\mu, \sigma^2)$. $p(\mathbf{z})$ is the prior on the latent space, modeled as the standard normal distribution $\mathcal{N}(0, I)$. The second term of (1) is the MSE loss between the raw and reconstructed images ($\mathbf{X}, d_{BEV}(\mathbf{z})$). The parameter β provides a trade-off between these two types of losses.

In this work, we set $\beta = 0.01$ and $\mathbf{z} \in \mathbb{R}^{512}$. We implement the VAE based on the ResNet18 architecture [40], where the decoder uses a combination of upsampling and convolutions for image reconstruction. Note the parameters of VAE are fixed during further policy training for stable performance [13], [38]. Some examples of the trained VAE network are shown in Fig. 5, from which we can conclude that the latent vector \mathbf{z} can capture the context information in various driving scenes.

B. Graph Modeling of Driving Scenes

1) *Architecture:* As shown in Fig. 2, we use GAT to model the interaction among road agents during driving, which is composed of multiple graph layers. The input to the i -th layer is a set of node features, $\{\mathbf{h}_1^i, \mathbf{h}_2^i, \dots, \mathbf{h}_N^i\}$, $\mathbf{h}_k^i \in \mathbb{R}^{F^i}$, where N is the number of nodes (agents, including the ego-vehicle), and F^i is the dimension of features in each node. Then, information of each node k are propagated to the neighboring nodes \mathcal{N}_k and being used to update the node features via a self-attention mechanism, which produces the

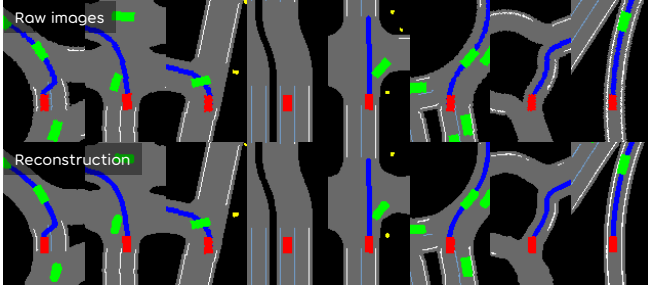


Fig. 5. Sample results of the trained VAE network. The first row shows the original input images and the second row shows the reconstructed images.

output of the layer:

$$\mathbf{h}_k^{i+1} = \sigma\left(\sum_{j \in \mathcal{N}_i} \alpha_{kj}(\mathbf{h}_k^i, \mathbf{h}_j^i) \mathbf{W} \mathbf{h}_j^i\right), \quad (2)$$

where $\sigma(\cdot)$ is the nonlinear activation function, e.g., ReLU; $\mathbf{W} \in \mathbb{R}^{F^{i+1} \times F^i}$ is a shared weight matrix to be applied to each node for expressive feature transformation; $\alpha_{kj}(\cdot, \cdot)$ means the importance of node j to node k , which is the normalized attention coefficients computed with shared weight vector $\bar{\mathbf{a}} \in \mathbb{R}^{2F^{i+1}}$:

$$\alpha_{kj}(\mathbf{h}_k^i, \mathbf{h}_j^i) = \frac{\exp(\sigma(\bar{\mathbf{a}}^T [\mathbf{W} \mathbf{h}_k^i || \mathbf{W} \mathbf{h}_j^i]))}{\sum_{m \in \mathcal{S}_k} (\sigma(\bar{\mathbf{a}}^T [\mathbf{W} \mathbf{h}_k^i || \mathbf{W} \mathbf{h}_m^i]))}, \quad (3)$$

where $||$ represents the concatenation operation. Furthermore, We follow the *multi-head attention* method in [27] to stabilize the learning process. Specifically, S^i independent graph networks execute the transformation of (2) and their features are concatenated to produce the output of the i -th layer:

$$\mathbf{h}_k^{i+1} = \big\|_{s=1}^{S^i} \sigma\left(\sum_{j \in \mathcal{N}_i} \alpha_{kj}^s(\mathbf{h}_k^i, \mathbf{h}_j^i) \mathbf{W}^s \mathbf{h}_j^i\right). \quad (4)$$

For the final layer, we employ *averaging* among multiple heads rather than concatenation.

2) *Details*: In this work, we adopt a two-layer GAT and set $S^1, S^2 = 5$, $F^1, F^2 = 256$. The input features \mathcal{C} include motion state information for each node (road agent) in the ego-vehicle's local coordinate. For node $k \in \{1, 2, \dots, N\}$, the input feature is a 10-dimensional vector:

$$\mathbf{c}_k = \{x, y, d, \psi, vx, vy, ax, ay, w, l\}, \quad (5)$$

which includes its location (x, y) , distance to the ego-vehicle (d) , yaw angle (ψ) , velocity (vx, vy) , acceleration (ax, ay) and size (width w and length l). In the spirit of [2], we first pass each node state $\mathbf{c}_k \in \mathcal{C}$ through a multilayer perceptron (MLP) to produce a feature vector $\mathbf{e}_k \in \mathbb{R}^{128}$ for sufficient expressive power. For context-aware graph modeling, we then concatenate \mathbf{e}_k with \mathbf{z} derived from the VAE introduced in Section IV-A, to generate the mixed vector \mathbf{g}_k . Then the set $\{\mathbf{g}_k\}$ are sent to GAT to output the final aggregated feature $\mathbf{h}_k^o \in \mathbb{R}^{256}$, which represents the internal interactions on each node k . We are interested in the result \mathbf{h}_1^o of the first node, which represents the influence on the ego-vehicle.

C. Task-relevant Feature Embedding

In addition to the interaction feature \mathbf{h}_1^o derived from the above section, we also need task-relevant information of the ego-vehicle to achieve mannered goal-directed self-driving, which is composed of two other feature vectors. The first vector $\mathbf{m} \in \mathbb{R}^{13}$ describes the ego-motion as follows:

$$\mathbf{m} = \{\tau_s, \tau_t, \tau_b, v_{lim}, vx, vy, ax, ay, e_v, e_{cte}, e_{heading}, F_l, F_r\}, \quad (6)$$

where τ_s, τ_t and τ_b indicate the current control command of the ego-vehicle: steering angle, throttle and brake. v_{lim} means the traffic speed limit, e_v means the difference between v_{lim} and current vehicle speed, e_{cte} is the cross track error between the vehicle location and the reference route, and $e_{heading}$ is the heading angle error calculated with vector field guidance [41]. $F_{l(r)}$ is a binary indicator of the lane marking on the left (right) side of the ego-vehicle, which is set to 1 if the lane marking is crossable (e.g., a broken line), and set to 0 otherwise (e.g., a solid line).

The second vector is a route vector $G \in \mathbb{R}^{150}$:

$$G = \{(x_k, y_k) \mid 1 \leq k \leq 75\} \subset G_f, \quad (7)$$

where G_f is the full high-level route from the start point to the destination. During navigation, we down-sample G_f into local relevant route G based on the ego-vehicle's location. Specifically, the first waypoint (x_1, y_1) in G is the closest waypoint in G_f to the current vehicle location, and the distance of every two adjacent points is 0.4 m. Note the redundancy of route information in G and BEV is meaningful, where the state vector here provides more specific waypoint locations for the vehicle to follow, while the route mask of BEV can indicate if there are any obstacles on conflicting lanes of planned routes, as well as encode traffic light information.

Finally, we adopt three MLPs to transform \mathbf{m} , G and \mathbf{h}_1^o separately into feature vectors $f_m, f_G, f_h \in \mathbb{R}^{1024}$ for further processing.

D. Driving Policy Training

With components defined above, in this section we introduce the policy training method in terms of imitation learning. Specifically, the feature vectors f_m, f_G, f_h derived in Section IV-C are first concatenated and then processed with a MLP to produce the output. To reduce the burden of control [15] and improve the policy generalization performance [19], we adopt a mid-level output representation indicating the target speed v_T and course angle θ_T rather than direct vehicle control commands (e.g., steering and throttle). We then use L1 loss in terms of v_T and θ_T to train the policy. These mid-level indicators are translated by a PID controller to generate the device-level control commands, i.e., steering, throttle and brake. For implementation, to bound the range of v_T and θ_T , we regress two scalars of target speed ($\kappa_v \in [0, 1]$) and course angle ($\kappa_c \in [-1, 1]$). Then the target control values can be computed by the following equations:

$$v_T = v_{lim} \times \kappa_v, \quad \theta_T = 90^\circ \times \kappa_c. \quad (8)$$

TABLE I

CLOSED-LOOP DRIVING RESULTS OF DIFFERENT MODELS ON SIX MAPS IN CARLA. SR MEANS THE SUCCESS RATE (%), AND DS MEANS THE DRIVING SCORE. LARGER NUMBERS ARE BETTER. THE BOLD FONT HIGHLIGHTS THE BEST RESULTS IN EACH COLUMN.

Town Name	Training Towns								Unseen Towns			
	Town03		Town05		Town06		Town07		Town04		Town10	
	<i>urban</i>		<i>urban</i>		<i>highway</i>		<i>rural</i>		<i>mixed</i>		<i>urban</i>	
Metrics	SR	DS	SR	DS	SR	DS	SR	DS	SR	DS	SR	DS
MLP	64.8	0.73	72.5	0.79	67.0	0.74	74.2	0.80	59.8	0.69	52.8	0.51
GAT	76.8	0.79	78.0	0.83	72.5	0.79	82.0	0.86	71.8	0.77	75.2	0.69
GCN (U)	77.5	0.81	79.0	0.83	71.5	0.77	75.0	0.81	66.5	0.73	74.2	0.66
GCN (D)	74.0	0.78	78.0	0.82	70.0	0.77	80.5	0.85	65.2	0.72	69.2	0.63
BEV	19.2	0.32	31.5	0.46	26.2	0.38	48.8	0.60	29.8	0.42	12.0	0.22
BEV (-G)	18.2	0.31	30.5	0.44	27.8	0.38	37.2	0.50	26.8	0.38	8.2	0.17
DiGNet (CTL)	74.5	0.76	80.8	0.83	72.8	0.78	78.5	0.82	69.0	0.74	67.2	0.58
DiGNet (<i>ours</i>)	77.5	0.81	78.8	0.83	75.5	0.81	83.2	0.87	76.0	0.81	73.5	0.66

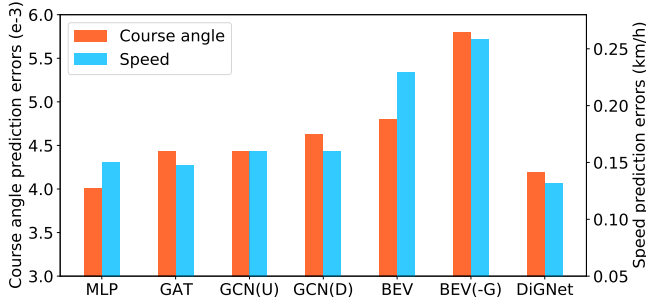


Fig. 6. Open loop prediction errors of different models.

V. EXPERIMENTS AND DISCUSSION

A. Training setup

We train our network DiGNet on the collected dataset introduced in Section III-B. The split ratio of training, validation and testing set is set to 17:1:2, leading to 240K training samples. We set the batch size to 256, and use the Adam optimizer with a learning rate of 0.0001. For comparison, we also train seven other baselines on the same training set. These baselines can be divided into three categories:

1) *state*-based networks used for crowd robot navigation in [2], [34], [35], commonly implemented with GNNs.

- GAT takes as input $\{\mathcal{C}, G, \mathbf{m}\}$ to produce the target control scalars $\{\kappa_v, \kappa_\theta\}$. Its difference to our proposed method is the non-use of the context embedding \mathbf{z} .
- GCN (U) is similar to GAT but adopts a two-layer GCN rather than GAT to process the node features \mathcal{C} . We refer to the baseline *U-GCNRL* introduced in [2] and set the adjacency matrix of GCN with uniform weights.
- GCN (D) is similar to GCN (U) but uses distance-related weights in its adjacency matrix. It adopts a straightforward intuition that obstacles closer to the ego-vehicle should exert a stronger influence. This network follows the idea of *D-GCNRL* introduced in [2].
- MLP is similar to GCN (D) but uses MLP rather than GNNs to process the node features. This baseline is added to verify the advantage of GNN to handle interactions among different nodes.

2) *Image pixel*-based methods [1], [15] that use BEV representations for autonomous driving.

- BEV takes as input $\{\mathbf{z}, G, \mathbf{m}\}$ to produce the output.
- BEV (-G) removes the local route information G from BEV.

3) The third category is a variant of our method, which has different output representations.

- DiGNet (CTL) directly generates device-level control commands (i.e., steering, throttle and brake) rather than the mid-level target speed/angle scalars as our method. Accordingly, we adopt L1 loss in terms of control commands for training.

B. Open-Loop Evaluation

In this section, we evaluate different models on the test set of 28,000 samples and compute their average L1 error between the prediction and ground-truth values¹. The results are shown in Fig. 6. It can be seen that the *state*-based methods perform better than the *pixel*-based methods with lower errors, of which the MLP achieves the lowest course angle prediction error. By merging the benefits of both, our model DiGNet achieves the lowest speed prediction error and the second lowest course angle prediction error.

The superiority of MLP than the GNN methods in this part seems counterfactual, as we know that GNNs are more suitable to handle node interactions. In fact, as reported in [15], [17], the offline evaluation of driving models may not reflect the real driving performance. Therefore, in the following section, we will conduct more closed-loop evaluations.

C. Closed-Loop Evaluation

1) *Evaluation benchmark*: In this section, we evaluate different models with closed-loop driving tasks on six maps in CARLA, including two unseen maps Town04 and Town10. Town04 is a mixed environment with highway roads and a small town. In each map, we set 10 routes for the ego-vehicle to drive, and each route includes 40 driving episodes.

¹Since the model DiGNet(CTL) uses different output representations, we do not compare its prediction error with other models in this section.

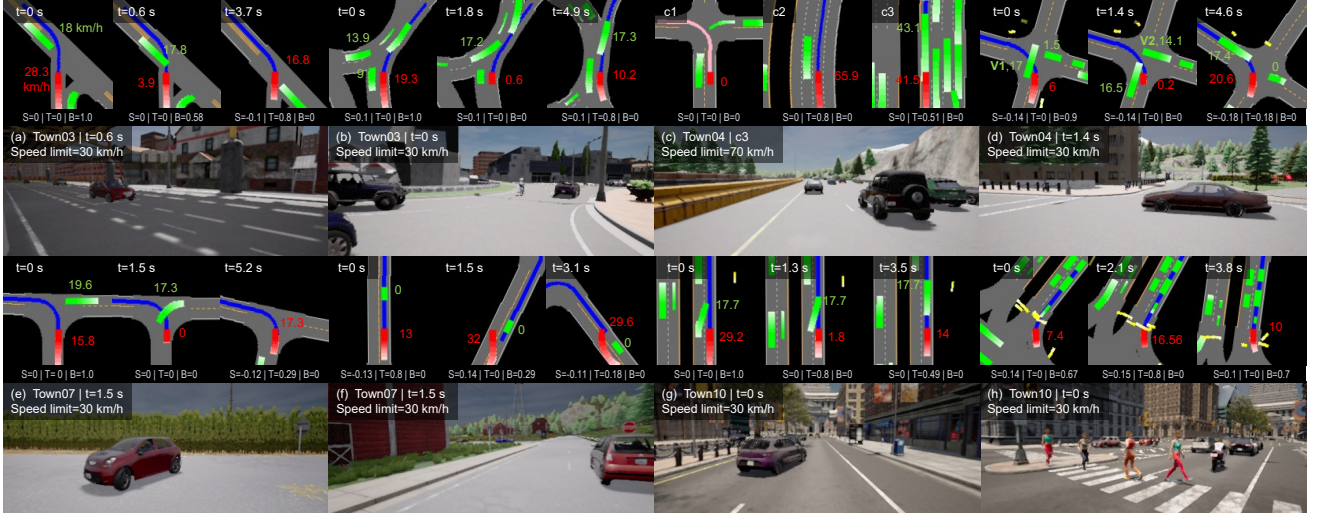


Fig. 7. Closed-loop evaluation results of our DiGNet. We show several driving clips with BEV and FPV images in four maps covering urban, rural and highway areas, where Town04 and Town10 are unseen maps in the training set. For better visualization, we set the color of route to pink if traffic light turns to red, otherwise to blue. In addition, we render trajectories in the past 1.5 s for road agents, where the lighter color indicates the more distant historical location. We also label the speed of key vehicles (ego-vehicle in red and other vehicles in green), and the output control commands (S-steer, T-throttle, B-brake) for better understanding. The range of steering is $[-1,1]$, while for throttle and brake the range is $[0,1]$. The sample driving behaviors are: slowing down when turning at (a,d,e) intersections or (b) roundabouts for collision avoidance, (c1) stopping at intersections with red traffic light, (c2,c3) high-speed driving and vehicle-following on highways, (f) driving around a parked vehicle on narrow roads, (g) slowing down when another vehicle in front suddenly changes lanes to the lane of ego-vehicle, and (h) crowd-aware safe driving among multiple pedestrians, including slowing down for collision avoidance ($t=0$ s) and continuing to drive when no pedestrians blocking ways ($t=2.1$ s).

For each episode, we set random number of vehicles (10-300) and pedestrians (10-90) roaming around the map, which are also spawned with random properties (i.e., speeds, destinations) at random positions. Due to such randomness, the environmental dynamics of seen maps is also different from the training dataset. Finally, we conduct 19,200 episodes to thoroughly evaluate 8 driving models (over 7,500 km).

2) *Evaluation Metrics*: We use two metrics to measure the driving performance on each map. The first is success rate (SR). An episode is considered to be successful if the agent reaches a certain goal without any collision within a time limit. The second metric is driving score (DS) defined as $\frac{1}{n} \sum_i R_i P_i$, where n stands for the number of episodes (400 in this work), R_i is the percentage of completion of the route in the i -th episode, and P_i is the collision penalty of the i -th episode (set to 0.5 if collision happens, otherwise set to 1).

3) *Quantitative Analysis*: Table I shows the quantitative evaluation results. We can first see that although MLP has smaller or similar prediction errors than GNN-based methods, its closed-loop performance is much worse. For example, the SR in Town10 of MLP is only 52.8%, which is much lower than the GNN-based methods (67.2%-75.2%). Second, the redundant route information in BEV input and G is valuable, as we can see that BEV(- G) generally has lower SR and DS than BEV. This validates with our statements in Section IV-C. Third, using BEV images only for interaction modeling is insufficient, since the highest SR of BEV (48.8%) is even much lower than the lowest SR of GNN-based methods (67.2%, DiGNet (CTL)). Fourth, our proposed method DiGNet achieve the best overall results by integrating both the pixel and state information with VAE and GAT. Finally, DiGNet achieves higher SR and DS than

DiGNet (CTL) in all maps, which validates the benefits of generalization improvement of our mid-level outputs (κ_v, κ_c).

4) *Qualitative results*: Fig. 7 shows the qualitative results of DiGNet. We can see that our model can safely and efficiently drive in diverse dynamic environments with different road structures (roundabouts, intersections, highways, etc.) and traffic scenarios, whilst obeying traffic rules such as speed limits and traffic lights. For example, in Fig. 7-(d), our model is turning left at an intersection, however, vehicle V1 is coming from the opposite direction without slowing down (speed=17 km/h). Our model timely loses the throttle and applies a large brake (0.9) to avoid collisions. When $t=1.4$ s, another vehicle V2 is coming from the right side at a speed of 14.1 km/h. Our model continues to wait until it is safe to speed up ($t=4.6$ s). More live driving behaviors are shown in the supplementary videos².

VI. CONCLUSION AND FUTURE WORK

This work has developed a context-aware graph-based deep navigation network named DiGNet to realize scalable self-driving in generic traffic scenarios. The core idea is first using VAE to encode semantic driving contexts into concise and informative latent vectors, which can then be incorporated with state vectors (e.g., locations and speeds) into GNNs to model the complex interactions among road agents. The large-scale closed-loop evaluation results of DiGNet w.r.t. the other seven models confirm that our method can complement pixel and state information to handle complex driving situations, and achieve the best overall performance in both seen and unseen environments. In the future, we aim to further test our method in real-world driving scenarios.

²<https://sites.google.com/view/dignet-self-driving/>

REFERENCES

- [1] J. Chen, B. Yuan, and M. Tomizuka, "Deep imitation learning for autonomous driving in generic urban scenarios with enhanced safety," *2019 IEEE/RSJ International Conference on Intelligent Robots and Systems (IROS)*, pp. 2884–2890, 2019.
- [2] Y. Chen, C. Liu, B. Shi, and M. Liu, "Robot navigation in crowds by graph convolutional networks with attention learned from human gaze," *IEEE Robotics and Automation Letters*, vol. 5, pp. 2754–2761, 2020.
- [3] J. Leonard *et al.*, "A perception-driven autonomous urban vehicle," *J. Field Robot.*, vol. 25, no. 10, pp. 727–774, 2008.
- [4] E. D. Dickmanns, "The development of machine vision for road vehicles in the last decade," in *Intelligent Vehicle Symposium, 2002. IEEE*, vol. 1. IEEE, 2002, pp. 268–281.
- [5] B. Paden, M. Cáp, S. Z. Yong, D. S. Yershov, and E. Frazzoli, "A survey of motion planning and control techniques for self-driving urban vehicles," *IEEE Transactions on Intelligent Vehicles*, vol. 1, pp. 33–55, 2016.
- [6] D. González, J. Pérez, V. M. Montero, and F. Nashashibi, "A review of motion planning techniques for automated vehicles," *IEEE Transactions on Intelligent Transportation Systems*, vol. 17, pp. 1135–1145, 2016.
- [7] W. Zeng, W. Luo, S. Suo, A. Sadat, B. Yang, S. Casas, and R. Urtasun, "End-to-end interpretable neural motion planner," *2019 IEEE/CVF Conference on Computer Vision and Pattern Recognition (CVPR)*, pp. 8652–8661, 2019.
- [8] Y. Koren and J. Borenstein, "Potential field methods and their inherent limitations for mobile robot navigation," *Proceedings. 1991 IEEE International Conference on Robotics and Automation*, pp. 1398–1404 vol.2, 1991.
- [9] O. Khatib, "Real-time obstacle avoidance for manipulators and mobile robots," *Proceedings. 1985 IEEE International Conference on Robotics and Automation*, vol. 2, pp. 500–505, 1985.
- [10] S. Kuutti, R. Bowden, Y. Jin, P. Barber, and S. Fallah, "A survey of deep learning applications to autonomous vehicle control," *IEEE Transactions on Intelligent Transportation Systems*, pp. 1–22, 2020.
- [11] P. Cai, S. Wang, Y. Sun, and M. Liu, "Probabilistic end-to-end vehicle navigation in complex dynamic environments with multimodal sensor fusion," *IEEE Robotics and Automation Letters*, vol. 5, pp. 4218–4224, 2020.
- [12] D. Chen, B. Zhou, V. Koltun, and P. Krähenbühl, "Learning by cheating," in *CoRL*, 2019.
- [13] E. Ohn-Bar, A. Prakash, A. Behl, K. Chitta, and A. Geiger, "Learning situational driving," *2020 IEEE/CVF Conference on Computer Vision and Pattern Recognition (CVPR)*, pp. 11 293–11 302, 2020.
- [14] P. Cai, X. Mei, L. Tai, Y. Sun, and M. Liu, "High-speed autonomous drifting with deep reinforcement learning," *IEEE Robotics and Automation Letters*, vol. 5, pp. 1247–1254, 2020.
- [15] M. Bansal, A. Krizhevsky, and A. Ogale, "Chauffeurnet: Learning to drive by imitating the best and synthesizing the worst," in *Proc. Robot.: Sci. Syst.*, June 2019.
- [16] F. Codevilla, M. Müller, A. López, V. Koltun, and A. Dosovitskiy, "End-to-end driving via conditional imitation learning," in *2018 IEEE International Conference on Robotics and Automation (ICRA)*. IEEE, 2018, pp. 1–9.
- [17] F. Codevilla, E. Santana, A. M. López, and A. Gaidon, "Exploring the limitations of behavior cloning for autonomous driving," in *Proceedings of the IEEE International Conference on Computer Vision*, 2019, pp. 9329–9338.
- [18] L. Tai, P. Yun, Y. Chen, C. Liu, H. Ye, and M. Liu, "Visual-based autonomous driving deployment from a stochastic and uncertainty-aware perspective," *2019 IEEE/RSJ International Conference on Intelligent Robots and Systems (IROS)*, pp. 2622–2628, 2019.
- [19] P. Cai, Y. Sun, H. Wang, and M. Liu, "VTGNet: A vision-based trajectory generation network for autonomous vehicles in urban environments," *IEEE Transactions on Intelligent Vehicles*, pp. 1–1, 2020.
- [20] A. Kendall, J. Hawke, D. Janz, P. Mazur, D. Reda, J.-M. Allen, V.-D. Lam, A. Bewley, and A. Shah, "Learning to drive in a day," *2019 International Conference on Robotics and Automation (ICRA)*, pp. 8248–8254, 2019.
- [21] H. Xu, Y. Gao, F. Yu, and T. Darrell, "End-to-end learning of driving models from large-scale video datasets," *2017 IEEE Conference on Computer Vision and Pattern Recognition (CVPR)*, pp. 3530–3538, 2017.
- [22] P. Wang, C.-Y. Chan, and A. D. L. Fortelle, "A reinforcement learning based approach for automated lane change maneuvers," *2018 IEEE Intelligent Vehicles Symposium (IV)*, pp. 1379–1384, 2018.
- [23] H. Porav and P. Newman, "Imminent collision mitigation with reinforcement learning and vision," *2018 21st International Conference on Intelligent Transportation Systems (ITSC)*, pp. 958–964, 2018.
- [24] Z. Cao, E. Biyik, W. Z. Wang, A. Raventos, A. Gaidon, G. Rosman, and D. Sadigh, "Reinforcement learning based control of imitative policies for near-accident driving," *ArXiv*, vol. abs/2007.00178, 2020.
- [25] H. Chae, C. M. Kang, B. Kim, J. Kim, C. C. Chung, and J. W. Choi, "Autonomous braking system via deep reinforcement learning," in *2017 IEEE 20th International Conference on Intelligent Transportation Systems (ITSC)*. IEEE, 2017, pp. 1–6.
- [26] J. Woo and N. Kim, "Collision avoidance for an unmanned surface vehicle using deep reinforcement learning," *Ocean Engineering*, vol. 199, p. 107001, 2020.
- [27] P. Veličković, G. Cucurull, A. Casanova, A. Romero, P. Liò, and Y. Bengio, "Graph Attention Networks," *International Conference on Learning Representations*, 2018.
- [28] D. P. Kingma and M. Welling, "Auto-encoding variational bayes," in *ICLR*, Y. Bengio and Y. LeCun, Eds., 2014.
- [29] J. Zhang, L. Tai, P. Yun, Y. Xiong, M. Liu, J. Boedecker, and W. Burgard, "Vr-goggles for robots: Real-to-sim domain adaptation for visual control," *IEEE Robotics and Automation Letters*, vol. 4, pp. 1148–1155, 2019.
- [30] W. Zeng, S. Wang, R. Liao, Y. Chen, B. Yang, and R. Urtasun, "Dsdnet: Deep structured self-driving network," in *Proceedings of the European Conference on Computer Vision (ECCV)*, 2020.
- [31] A. Sadat, S. Casas, M. Ren, X. Wu, P. Dhawan, and R. Urtasun, "Perceive, predict, and plan: Safe motion planning through interpretable semantic representations," in *Proceedings of the European Conference on Computer Vision (ECCV)*, 2020.
- [32] S. Yang, W. Wang, C. Liu, and W. Deng, "Scene understanding in deep learning-based end-to-end controllers for autonomous vehicles," *IEEE Transactions on Systems, Man, and Cybernetics: Systems*, vol. 49, pp. 53–63, 2019.
- [33] M. Defferrard, X. Bresson, and P. Vandergheynst, "Convolutional neural networks on graphs with fast localized spectral filtering," in *NIPS*, 2016.
- [34] C. Chen, S. Hu, P. Nikdel, G. Mori, and M. Savva, "Relational graph learning for crowd navigation," *arXiv preprint arXiv:1909.13165*, 2019.
- [35] L. Manso, R. R. Jorvekar, D. R. Faria, P. Bustos, and P. Bachiller, "Graph neural networks for human-aware social navigation," *ArXiv*, vol. abs/1909.09003, 2019.
- [36] A. Dosovitskiy, G. Ros, F. Codevilla, A. Lopez, and V. Koltun, "CARLA: An open urban driving simulator," in *Proc. 1st Annu. Conf. Robot Learn.*, vol. 78, Nov 2017, pp. 1–16.
- [37] J. Zhang, L. Tai, P. Yun, Y. Xiong, M. Liu, J. Boedecker, and W. Burgard, "Vr-goggles for robots: Real-to-sim domain adaptation for visual control," *IEEE Robotics and Automation Letters*, vol. 4, no. 2, pp. 1148–1155, 2019.
- [38] J. Chen, B. Yuan, and M. Tomizuka, "Model-free deep reinforcement learning for urban autonomous driving," *2019 IEEE Intelligent Transportation Systems Conference (ITSC)*, pp. 2765–2771, 2019.
- [39] I. Higgins, L. Matthey, A. Pal, C. Burgess, X. Glorot, M. Botvinick, S. Mohamed, and A. Lerchner, "beta-vae: Learning basic visual concepts with a constrained variational framework," in *ICLR*, 2017.
- [40] K. He, X. Zhang, S. Ren, and J. Sun, "Deep residual learning for image recognition," *2016 IEEE Conference on Computer Vision and Pattern Recognition (CVPR)*, pp. 770–778, 2016.
- [41] D. Nelson, D. B. Barber, T. McLain, and R. Beard, "Vector field path following for miniature air vehicles," *IEEE Transactions on Robotics*, vol. 23, pp. 519–529, 2007.